Letter

Exploring possible Fermi surface nesting and the nature of heavy quasiparticles in the spin-triplet superconductor candidate $CeRh_2As_2$

Bo Chen,[1] Hao Liu,[1] Qi-Yi Wu,[1] Chen Zhang,[1] Xue-Qing Ye,[1] Yin-Zou Zhao,[1] Jiao-Jiao Song,[1] Xin-Yi Tian,[1] Ba-Lei Tan,[1] Zheng-Tai Liu,[2] Mao Ye,[2] Zhen-Hua Chen,[2] Yao-Bo Huang,[2] Da-Wei Shen,[3] Ya-Hua Yuan,[1] Jun He,[1] Yu-Xia Duan,[1] and Jian-Qiao Meng[1,*]

[1]*School of Physics, Central South University, Changsha, Hunan 410083, China*

[2]*Shanghai Synchrotron Radiation Facility, Shanghai Advanced Research Institute, Chinese Academy of Sciences, Shanghai 201204, China*

[3]*National Synchrotron Radiation Laboratory and School of Nuclear Science and Technology, University of Science and Technology of China, Hefei, Anhui 230026, China*

(Received 15 March 2024; revised 10 July 2024; accepted 12 July 2024; published 26 July 2024)

In this Letter, we investigate the electronic structure of a spin-triplet superconductor candidate $CeRh_2As_2$ using high-resolution angle-resolved photoemission spectroscopy and density functional theory calculations. Notably, possible Fermi surface nesting hints at connections to magnetic excitation or quadrupole density wave phenomena, elucidating the superconducting mechanisms. Measured band structures reveal primarily localized $4f$ electrons, with minor itinerant contributions. Additionally, a transition from localized to itinerant behavior and significant c-f hybridization anisotropy underscore the role of f electrons in shaping electronic properties. These findings deepen our understanding of $CeRh_2As_2$'s unconventional superconductivity and magnetism. Further exploration promises advances in superconductivity research.

DOI: 10.1103/PhysRevB.110.L041120

$CeRh_2As_2$, a recently discovered heavy-fermion (HF) superconductor, has attracted considerable attention due to its exceptional characteristics [1]. With decreasing temperature, $CeRh_2As_2$ undergoes a potential quadrupole density wave (QDW) phase transition at $T_0 \approx 0.4$–0.5 K [2,3], succeeded by a superconducting transition at $T_c \approx 0.3$–0.4 K [1–6], and finally an antiferromagnetic (AFM) phase transition at the Néel temperature $T_N \approx 0.25$ K, coexisting with superconductivity within its superconducting phase [4,5]. Multiple field-induced superconducting phases have been observed, with the transition between two different superconducting phases suggested to be a spin-singlet (even-parity) to spin-triplet (odd-parity) transition [1]. Despite its remarkably low superconducting transition temperature, $CeRh_2As_2$ displays an unusually high superconducting upper critical field, reaching up to 14 T [1], surpassing the Pauli limit. This multiphase superconductivity in HF compounds is rare, as most unconventional superconductors typically exhibit a single superconducting phase [7,8]. Moreover, in systems where superconductivity and magnetism coexist or compete, the superconducting phase generally lacks AFM order parameters, with T_N consistently exceeding the superconducting temperature T_c.

The distinct physical properties of $CeRh_2As_2$, uncovered through numerous experimental [1–6] and theoretical [9–17] studies, stem from its unique local noncentrosymmetric crystal structure. Unlike other noncentrosymmetric compounds such as $CeRhSi_3$ [18], $CePt_3Si$ [19], and $CeCoGe_3$ [20], which showcase a combination of odd-parity and even-parity states without displaying multiphase superconductivity, $CeRh_2As_2$ exhibits multiphase superconductivity. This distinction renders $CeRh_2As_2$ an excellent model system for investigating how crystal structures lacking local central symmetry can influence unconventional superconductivity and magnetic interactions, thus elucidating the complex interplay between these phenomena [4]. For instance, the locally symmetry-lacking structure of $CeRh_2As_2$ may induce a significant Rashba-like spin-orbit coupling (SOC) of the $4f$ and the conduction bands, a factor believed to be pivotal in the superconductivity parity transition [1,10,11].

Despite numerous experimental [1–6] and theoretical [9–17] efforts, the mechanism of superconductivity in $CeRh_2As_2$ remains controversial. The observation of multiphase superconductivity in the spin-triplet candidate $5f$-HF UTe_2 [21–23] underscores the pivotal role of spin fluctuations in its unconventional superconducting state. Similarly, spin fluctuations were proposed as a possible mechanism for superconductivity in $CeRh_2As_2$ [1]. The observed field-induced transition within the superconducting phase might arise from an even-odd parity effect driven by local noncentrosymmetricity at the Ce sites [1]. However, Machida's AFM ordering picture also provides a potential explanation, which is supported by neutron scattering data revealing quasi-two-dimensional (2D) AFM spin fluctuations with a wave vector of $\boldsymbol{q} = (\pi/a, \pi/a)$ [24]. Some studies suggest a close relationship between the Kondo effect and superconductivity in $CeRh_2As_2$ [16], contributing to the ongoing debate over the role of Kondo physics [2,10–15]. Specific heat measurements suggested that the heavy f electrons are involved in the superconducting transition [1]. The resistivity shows a characteristic hump at ∼40 K, and the magnetic entropy

*Contact author: jqmeng@csu.edu.cn

monotonically increases to reach the value $R\ln 4$ at 60 K, suggesting Kondo screening is active well above T_N and involving the two low-lying doublets with very close energy in the crystal electric field (CEF) state [2]. Angle-resolved photoemission spectroscopy (ARPES), a momentum-resolved technology, serves as an ideal tool to address these issues, identifying potential Fermi surface (FS) nesting required for magnetic excitation [24] and QDW, detecting band splitting caused by spin-orbit coupling (SOC), and elucidating the role played by f electrons.

In this Letter, we investigate the electronic structure of $CeRh_2As_2$, a spin-triplet superconductor candidate, using high-resolution ARPES measurements and density functional theory (DFT) calculations. We observe a possible FS nesting vector that aligns with magnetic excitation, potentially associated with QDW phenomena. Furthermore, the observed consistency between the measured FS topology and localized $4f$ electron calculations, along with the involvement of f electrons in shaping the FS as evidenced by on-resonance measurements, collectively suggest the dual nature of the $4f$ electrons.

In this study, high-quality single crystals of $CeRh_2As_2$ were grown via a Bi-flux method. ARPES measurements were conducted at the BL09U and BL03U beamlines of the Shanghai Synchrotron Radiation Facility (SSRF) using a Scienta DA30 analyzer under ultrahigh vacuum conditions ($<4\times10^{-11}$ mbar). All samples were cleaved *in situ* at ~11 K. FS topology was mapped by systematic measurements with varying photon energies ($h\nu = 48$–130 eV) for k_z (perpendicular) and constant photon energy ($h\nu = 70$ eV) for $k_\parallel$ (horizontal) directions. Experimental FS topology and band structures were compared with DFT calculations. Temperature-dependent on-resonance $4d \rightarrow 4f$ ($h\nu =$ 121 eV) ARPES spectra were applied to probe the nature of the Ce $4f$ electrons.

$CeRh_2As_2$ crystallizes in a centrosymmetric $CaBe_2Ge_2$-type tetragonal structure with the $P4/nmm$ space group (No. 129, D74h) [Fig. 1(a)] [25]. The Ce site lacks local inversion symmetry, while maintaining a global spatial inversion center. Positioned between two different RhAs block layers, this local inversion symmetry breaking at the Ce layer is considered crucial for $CeRh_2As_2$'s superconductivity. The bulk Brillouin zone (BZ) of $CeRh_2As_2$ and its projection onto the (001) surface BZ, including high-symmetry momentum points, are shown in Fig. 1(b). At 11 K, photon-energy-dependent normal scans was illustrated in Fig. 1(c). Although the intensity of the FSs varies with the photon energies, it behaves in three dimensions, as predicted by calculation (see Figs. S2 and S3 in the Supplemental Material for more data [26]). Additionally, as other studies [31–33], the FSs near the BZ center exhibit quasi-2D characteristics. Subsequently, an inner potential (V_0) of 16 eV was taken, consistent with findings from other studies [31–33], a common value in Ce-based HFs.

To search for the possible spin fluctuation required FS nesting vector $\boldsymbol{q} = (\pi/a, \pi/a)$, a constant photon energy k_x-k_y mapping was conducted using 70 eV photons at 11 K [Fig. 1(d)]. The high-intensity spots at the X' could possibly arise from a FS nesting that coincidentally shares the wave vector $\boldsymbol{q}$ required by AFM spin fluctuations [24], as indicated by the cyan double arrow, possibly accounting for the QDW

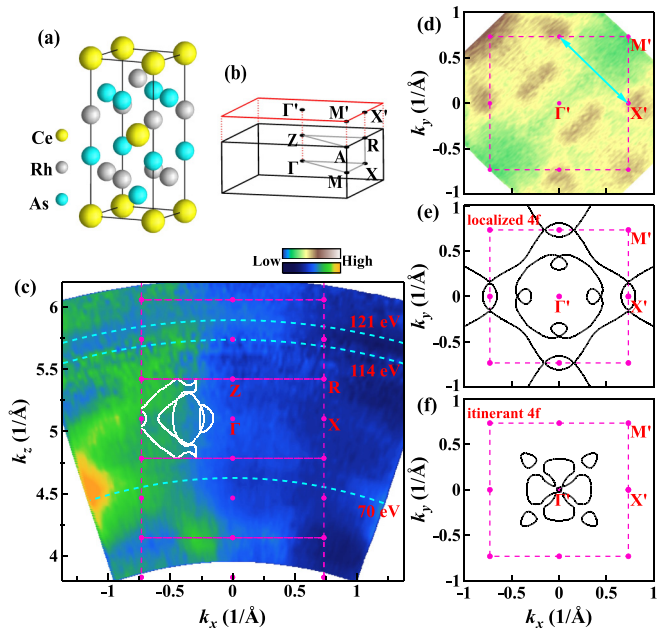

FIG. 1. FSs of $CeRh_2As_2$ at low temperature of 11 K. (a) Crystal structure of $CeRh_2As_2$. (b) 3D BZ (black) and projected surface BZ (red) of $CeRh_2As_2$, with high-symmetry momentum points marked (black dots). (c) Experimental 3D FS maps measured using $h\nu =$ 48–130 eV photons in 2 eV steps, in the ΓZRX plane. Final state arcs (cyan-dashed lines) for different photon energies are indicated. Gray curves depict calculated FS contours assuming localized $4f$ electrons (core electrons). (d) Constant photon energy k_x-k_y map taken with 70 eV photons. Photoemission intensities were integrated over an [−10 meV, 10 meV] energy window with respect to E_F. The cyan double arrow indicate the possible FS nesting vector $\boldsymbol{q}$. (e) and (f) Calculated 2D FS contours at $k_z = 0.5\pi/c$ [26], considering $4f$ electrons as localized $4f$ electrons (core electrons) and itinerant $4f$ electrons (valence electrons), respectively.

[2]. This observation aligns with findings from other ARPES studies [32]. Figures 1(e) and 1(f) depict the calculated FS at $k_z = 0.5\pi/c$, considering $4f$ electrons as core electrons (localized $4f$) and valence electrons (itinerant $4f$), respectively. The experimental FSs are inferred to be more consistent with the localized $4f$ DFT calculation. This finding reinforces the justification for treating $4f$ electrons as core electrons in nonresonant excitation studies. The FS shape calculated based on localized $4f$ electrons also supports the possibility of FS nesting with a wave vector $\boldsymbol{q}$ [Fig. 1(e)].

To investigate the properties of Ce $4f$ electrons, we conducted $4d \rightarrow 4f$ on-resonant ARPES measurements using 121 eV photons for resonance enhancement. Figures 2(a) and 2(b) compare off-resonance (114 eV) and on-resonance (121 eV) photoemission spectra at 11 K, along the Γ'-X' direction. In the off-resonance spectrum, contributions from Rh $4d$ and As $4p$ states create dispersive bands with non-f orbital character, corroborated by the angle-integrated energy distribution curve (EDC) (solid blue line) in Fig. 2(d). To facilitate comparison with DFT calculations, in Fig. 2(a), we have superimposed the experimental band structure with dispersions along the Γ'-X' direction calculated for localized $4f$ electrons (white-hashed lines), as the position measured by 114 eV

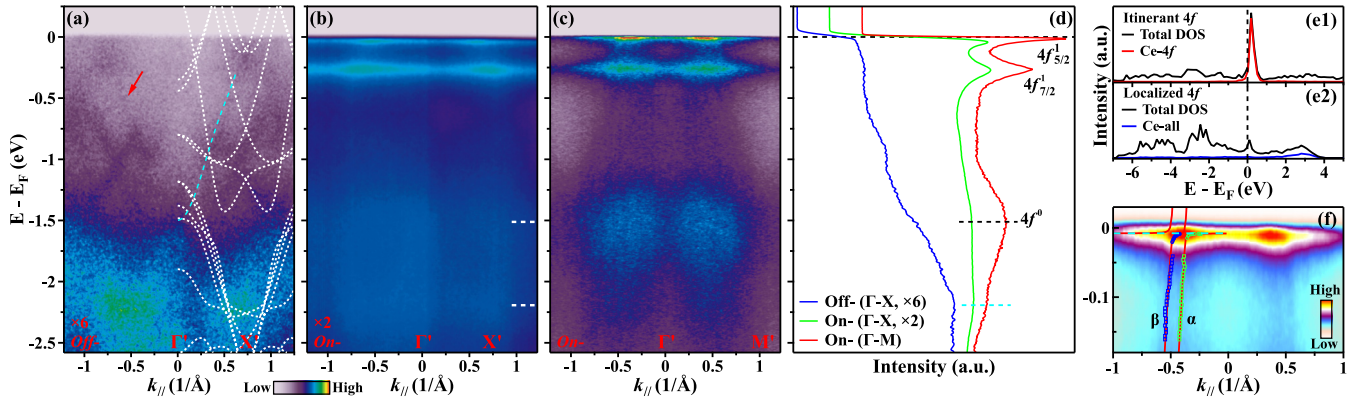

FIG. 2. Off-resonance and on-resonance ARPES data of $CeRh_2As_2$ at 11 K. (a) Off-resonance (114 eV) ARPES data along the Γ'-X' direction, with overlaid localized $4f$ calculation results along the Γ-X direction. (b) and (c) On-resonance (121 eV) ARPES data along the Γ'-X' and Γ'-M' directions, respectively. (d) Angle-integrated EDCs for data in (a)–(c). Positions of the $4f^1_{5/2}$, $4f^1_{7/2}$, and $4f^0$ states are indicated. (e1) and (e2) Calculated density of states (DOS) vs energy E for $CeRh_2As_2$, utilizing itinerant and localized $4f$ calculation methods, respectively. (f) Photoemission intensity near the E_F. The c-f hybridization is modeled using the periodic Anderson model. Squares and open circles represent positions of the conduction and hybridized f bands, respectively. The gray dashed line indicates the position of the f level.

photons corresponds to $k_z \sim 0$ [Fig. 1(c)]. While the calculated electronic structure generally aligns with the ARPES results, there are still some notable discrepancies. In particular, the Γ' centered electronlike dispersion (cyan-dashed line) indicated by the red arrow does not correspond to the theoretically calculated energy band. Considering its energy scale and momentum range, our observations suggest that Fermi surface folding with a wave vector of $\boldsymbol{q} = (\pi/a, \pi/a)$ folds an M'-centered electronlike band to the vicinity of the Γ' point (see Fig. S1 of the Supplemental Material [26]). This wave vector, which coincides with the magnetic excitation wave vector $\boldsymbol{q}$ revealed by Chen *et al.* [24], could be responsible for the QDW formation [2]. However, it is important to acknowledge that the electronlike band could also be caused by the folding of the surface band. While this observation provides valuable insight, it remains as an isolated data point. Definitive verification of the Fermi surface nesting mechanism requires high-precision mapping of the entire FS sheet, followed by calculation of the autocorrelation function from experimental data.

The on-resonance data exhibit a significant enhancement of Ce $4f$ states, attributed to strengthened Ce $4f$-electron photoconduction matrix elements. Observations reveal two strong heavy quasiparticle bands arising from the splitting of the $4f^1$ final state induced by SOC, as confirmed by the angle-integrated EDC (solid green line) in Fig. 2(d). A state approximately 0.27 eV below E_F is assigned to the $4f^1_{7/2}$ state, while the one proximite to E_F corresponds to the $4f^1_{5/2}$ state. Similar observations have been reported in previous studies on $CeRh_2As_2$ [31–33], and analogous structures have been documented in other Ce-based HF systems [34–42].

In Fig. 2(b), short dashed lines indicate the emergence of two broader peaks approximately 1.5 and 2.2 eV below E_F. The peak around 1.5 eV below E_F corresponds to the f^0 state, resulting from pure charge excitations of the trivalent Ce ion ($4f^1 \rightarrow 4f^0$) [34–42]. Meanwhile, the peak around 2.2 eV below E_F represents a shoulder of the f^0 state, reflecting hybridization spreading due to the structure in the valence band density of states [Fig. 2(a)] [34,35]. Remarkably, the intensity of the f^1 state surpasses that of the f^0 state, differing from observed patterns in $CePt_2In_7$ [36,37], $CeRhIn_5$ [36,38], Ce_2MIn_8 (M = Co, Rh, and Ir) [36,39], and others. This departure, consistent with observations in $CeCoIn_5$ [36,42] and $CeRh_6Ge_4$ [41], implies increased itinerancy of $4f$ electrons in $CeRh_2As_2$, according to the periodic Anderson model (PAM). However, DFT + U calculations ($U = 4$ or 0 eV for itinerant and localized $4f$, respectively) [Fig. 2(e)] suggest that the majority of Ce $4f$ states in $CeRh_2As_2$ are situated above E_F, with only a small fraction below E_F, which is a common feature in Ce-based HFs. Compared to Yb-based [43,44] and U-based [44–47] HFs, the f electrons in $CeRh_2As_2$ are more localized.

In Figs. 2(b) and 2(c), the significantly momentum-dependent intensity of the $4f^1_{5/2}$ and $4f^1_{7/2}$ states indicates pronounced c-f hybridization, suggesting the involvement of f electrons in forming the Fermi surface. Along the Γ'-X' direction, the $4f^1_{5/2}$ state exhibits weaker strength compared to the $4f^1_{7/2}$ state, while measurements along the Γ'-M' direction [Fig. 2(c)] reveal a contrasting trend. This disparity suggests anisotropic hybridization strength in momentum space, such as that due to the local noncentrosymmetric crystal structure of $CeRh_2As_2$.

Figure 2(f) presents the on-resonance spectral data along the Γ'-M' direction near E_F, highlighting the intersection between the conduction bands and the f band (see Fig. S5 in the Supplemental Material [26]). The data are normalized by the corresponding resolution-convoluted Fermi-Dirac function (RC-FDD). The unique observation of hybridization between the two adjacent conduction bands (α and β) and the f band is evident. Consistent with prior investigations [35,48], we analyzed the on-resonance spectra using a hybridization band model derived from the periodic Anderson model (PAM) [48,49]. In this framework, the hybridization results in (E^+) and lower (E^-) bands, expressed as

$$E^{\pm} = \frac{\varepsilon_f + \varepsilon_k \pm \sqrt{(\varepsilon_f - \varepsilon_k)^2 + 4|V_k|^2}}{2},$$

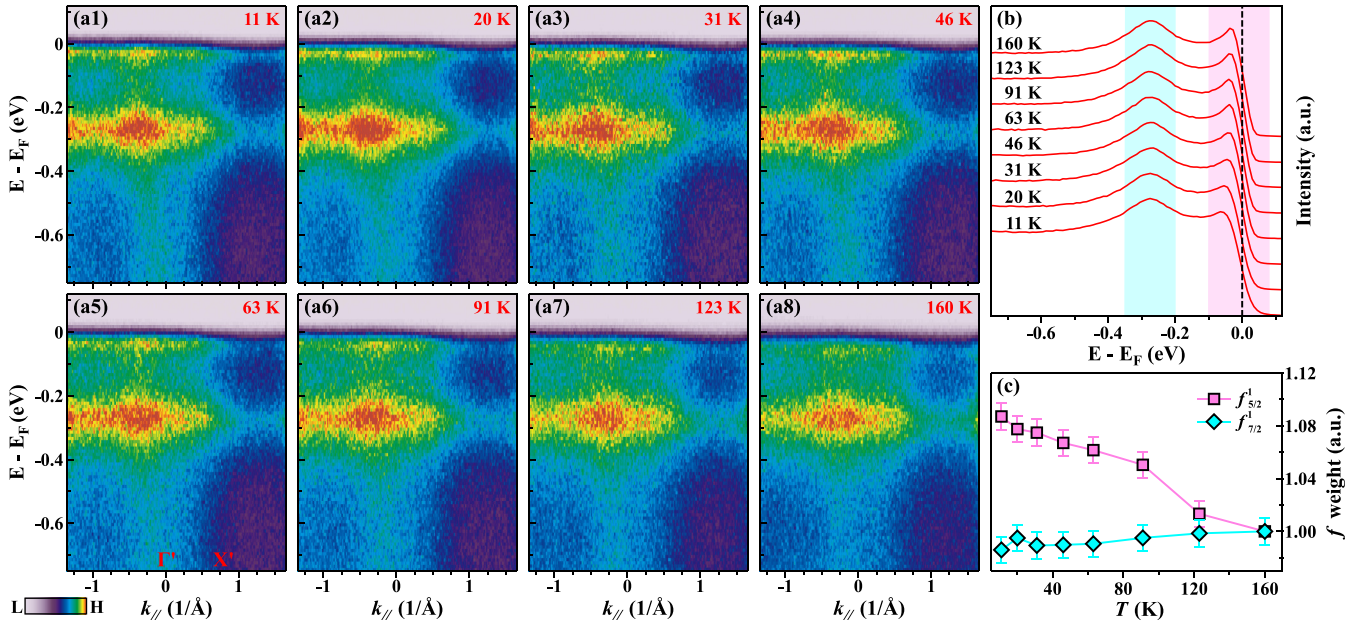

FIG. 3. Temperature-dependent evolution of heavy quasiparticle bands in $CeRh_2As_2$. (a) On-resonant band structure along the Γ'-X' direction at specified temperatures. (b) Angle-integrated EDCs over the entire angle range shown in (a) across different temperatures. (c) Normalized quasiparticle spectral weight as a function of temperature, normalized to the reference value at 160 K. Cyan and magenta markings signify spectral weight integrals corresponding to the highlighted regions in (b).

where ε_f denotes the renormalized f-level energy ($4f^1_{5/2}$ Kondo resonance state), ε_k represents the bare conduction band, and V_k symbolizes the renormalized hybridization (half of the direct hybridization gap) [48]. Fitting the model yields $\varepsilon_f = -9$ meV for both the α and β bands, with V_k values of 19 ± 3 and 8.5 ± 3 meV for the α and β bands, respectively. The obtained hybridization parameter value for the α band is consistent with values reported in a prior study ($\sim$20 meV) [31] and is similar to values found in other Ce-based heavy fermion compounds [35,42,50].

Understanding the properties f electrons in HF compounds and how they evolve with temperature is crucial for comprehending HF physics, especially in the compound $CeRh_2As_2$. Therefore, conducting a thorough investigation into c-f hybridization in $CeRh_2As_2$ is of paramount significance. Figure 3(a) presents the temperature-dependent on-resonance ARPES measurement along the Γ'-X' direction ranging from 11 to 160 K. Throughout this temperature range, the $4f^1_{5/2}$ and $4f^1_{7/2}$ states are observable. The intensity of the $4f^1_{5/2}$ states decreases with increasing temperature due to gradually weakened hybridization between the $4f$ and conduction electrons, while the intensity of the $4f^1_{7/2}$ states shows little change. However, even at 160 K, their intensity still exhibits significant momentum dependence, indicating ongoing c-f hybridization. Remarkably, the characteristics of the flat bands persist even at room temperature (see Fig. S4 in the Supplemental Material [26]), suggesting that the formation of the heavy quasiparticle band initiates at a temperature significantly higher than its Kondo temperature ($T_K \sim 30$ K) [1,2,6], consistent with observations in other Ce-based [38–42], Yb-based [43], and U-based [46,47] HF systems.

Figure 3(b) illustrates the temperature evolution of the angle-integrated EDCs within the measured momentum range shown in Fig. 3(a). As the temperature decreases, the peak of the $4f^1_{7/2}$ state remains nearly unchanged, while the peak of the $4f^1_{5/2}$ state becomes sharper. This observation suggests a broad temperature range crossover corresponding to the localized-to-itinerant transition of $4f$ electrons. While the enhanced hybridization temperature can be attributed to Kondo screening involving the excited crystal electric field (CEF) state, no visible serrated peak features caused by CEF splitting are observed in the EDCs, likely due to the limitations in our measurement's energy resolution.

Figure 3(c) provides a quantitative analysis of the evolution of f-electron spectral weight with temperature, normalized to the highest-temperature data. Within the experimental accuracy, the spectral weight of the $4f^1_{7/2}$ state shows no significant change with temperature. Conversely, the spectral weight of the $4f^1_{5/2}$ state gradually increases as temperature decreases, reaching nearly 10% in the displayed temperature range. These temperature-evolution behaviors are considerably weaker than those observed along the Γ'-M' direction [31], emphasizing the pronounced anisotropy of c-f hybridization. The observed slight increase may originate from its interaction with an electron-type conduction band along the Γ'-X' direction [Fig. 2(a)], where the band bottom closely approaches the $4f$ band. This band crossing and hybridization could lead to the emergence of additional hybridized state(s) slightly above E_F, contributing to the integrated intensity at higher temperatures and giving the impression of reduced temperature dependence of the $f^1_{5/2}$ state.

In summary, the investigation into the electronic structure of $CeRh_2As_2$, a spin-triplet superconductor, utilizing ARPES and DFT calculations, has yielded crucial insights into its multiphase superconductivity and antiferromagnetism. A

significant observation is the presence of possible Fermi surface nesting, suggesting a potential link to magnetic excitation or quadrupole density wave phenomena, thus illuminating the mechanisms driving the superconducting state. The measured band structures reveal the dual nature of $4f$ electrons, primarily localized with a minor itinerant contribution. Moreover, the broad transition from localized to itinerant behavior and the significant anisotropy in c-f hybridization underscore the importance of f electrons in shaping the electronic properties of $CeRh_2As_2$. These findings highlight the intricate interplay among electronic states in $CeRh_2As_2$, advancing our understanding of its unconventional superconductivity and magnetism.

This work was supported by the National Natural Science Foundation of China (Grant No. 12074436), the National Key Research and Development Program of China (Grant No. 2022YFA1604204), the Science and Technology Innovation Program of Hunan Province Grant No. (2022RC3068), and the Changsha Natural Science Foundation (Grant No. kq2208254). We are grateful for resources from the High Performance Computing Center of Central South University.

[1] S. Khim, J. F. Landaeta, J. Banda, N. Bannor, M. Brando, P. M. R. Brydon, D. Hafner, R. Küchler, R. Cardoso-Gil, U. Stockert, A. P. Mackenzie, D. F. Agterberg, C. Geibel, and E. Hassinger, Field-induced transition within the superconducting state of $CeRh_2As_2$, Science **373**, 1012 (2021).

[2] D. Hafner, P. Khanenko, E.-O. Eljaouhari, R. Küchler, J. Banda, N. Bannor, T. Lühmann, J. F. Landaeta, S. Mishra, I. Sheikin, E. Hassinger, S. Khim, C. Geibel, G. Zwicknagl, and M. Brando, Possible quadrupole density wave in the superconducting Kondo lattice $CeRh_2As_2$, Phys. Rev. X **12**, 011023 (2022).

[3] K. Semeniuk, D. Hafner, P. Khanenko, T. Lühmann, J. Banda, J. F. Landaeta, C. Geibel, S. Khim, E. Hassinger, and M. Brando, Decoupling multiphase superconductivity from normal state ordering in $CeRh_2As_2$, Phys. Rev. B **107**, L220504 (2023).

[4] M. Kibune, S. Kitagawa, K. Kinjo, S. Ogata, M. Manago, T. Taniguchi, K. Ishida, M. Brando, E. Hassinger, H. Rosner, C. Geibel, and S. Khim, Observation of antiferromagnetic order as odd-parity multipoles inside the superconducting phase in $CeRh_2As_2$, Phys. Rev. Lett. **128**, 057002 (2022).

[5] G. Chajewski and D. Kaczorowski, Discovery of magnetic phase transitions in heavy-fermion superconductor $CeRh_2As_2$, Phys. Rev. Lett. **132**, 076504 (2024).

[6] S. Onishi, U. Stockert, S. Khim, J. Banda, M. Brando, and E. Hassinger, Low-temperature thermal conductivity of the two-phase superconductor $CeRh_2As_2$, Front. Electron. Mater. **2**, 880579 (2022).

[7] G. R. Stewart, Heavy-fermion systems, Rev. Mod. Phys. **56**, 755 (1984).

[8] A. Pourret and G. Knebel, Driving multiphase superconductivity, Science **373**, 962 (2021).

[9] S. I. Kimura, J. Sichelschmidt, and S. Khim, Optical study of the electronic structure of locally noncentrosymmetric $CeRh_2As_2$, Phys. Rev. B **104**, 245116 (2021).

[10] K. Nogaki, A. Daido, J. Ishizuka, and Y. Yanase, Topological crystalline superconductivity in locally noncentrosymmetric, Phys. Rev. Res. **3**, L032071 (2021).

[11] D. C. Cavanagh, T. Shishidou, M. Weinert, P. M. R. Brydon, and D. F. Agterberg, Nonsymmorphic symmetry and field-driven odd-parity pairing in $CeRh_2As_2$, Phys. Rev. B **105**, L020505 (2022).

[12] D. Möckli and A. Ramires, Two scenarios for superconductivity in $CeRh_2As_2$, Phys. Rev. Res. **3**, 023204 (2021).

[13] D. Möckli and A. Ramires, Superconductivity in disordered locally noncentrosymmetric materials: An application to $CeRh_2As_2$, Phys. Rev. B **104**, 134517 (2021).

[14] E. G. Schertenleib, M. H. Fischer, and M. Sigrist, Unusual H-T phase diagram of $CeRh_2As_2$: The role of staggered noncentrosymmetricity, Phys. Rev. Res. **3**, 023179 (2021).

[15] A. Ptok, K. J. Kapcia, P. T. Jochym, J. Łażewski, A. M. Oleś, and P. Piekarz, Electronic and dynamical properties of $CeRh_2As_2$: Role of Rh_2As_2 layers and expected orbital order, Phys. Rev. B **104**, L041109 (2021).

[16] T. Hazra and P. Coleman, Triplet pairing mechanisms from Hund's-Kondo models: Applications to UTe_2 and $CeRh_2As_2$, Phys. Rev. Lett. **130**, 136002 (2023).

[17] K. Machida, Violation of Pauli-Clogston limit in the heavy-fermion superconductor $CeRh_2As_2$: Duality of itinerant and localized $4f$ electrons, Phys. Rev. B **106**, 184509 (2022).

[18] N. Kimura, K. Ito, K. Saitoh, Y. Umeda, H. Aoki, and T. Terashima, Pressure-induced superconductivity in noncentrosymmetric heavy-fermion $CeRhSi_3$, Phys. Rev. Lett. **95**, 247004 (2005).

[19] E. Bauer, G. Hilscher, H. Michor, C. Paul, E.-W. Scheidt, A. Gribanov, Y. Seropegin, H. Noël, M. Sigrist, and P. Rogl, Heavy fermion superconductivity and magnetic order in noncentrosymmetric $CePt_3Si$, Phys. Rev. Lett. **92**, 027003 (2004).

[20] R. Settai, I. Sugitani, Y. Okuda, A. Thamizhavel, M. Nakashima, Y. Ōnuki, and H. Harima, Pressure-induced superconductivity in $CeCoGe_3$ without inversion symmetry, J. Magn. Magn. Mater. **310**, 844 (2007).

[21] S. Ran, C. Eckberg, Q.-P. Ding, Y. Furukawa, T. Metz, S. R. Saha, I.-L. Liu, M. Zic, H. Kim, J. Paglione, and N. P. Butch, Nearly ferromagnetic spin-triplet superconductivity, Science **365**, 684 (2019).

[22] L. Jiao, S. Howard, S. Ran, Z. Wang, J. O. Rodriguez, M. Sigrist, Z. Wang, N. P. Butch, and V. Madhavan, Chiral superconductivity in heavy-fermion metal UTe_2, Nature (London) **579**, 523 (2020).

[23] D. Aoki, A. Nakamura, F. Honda, D. Li, Y. Homma, Y. Shimizu, Y. J. Sato, G. Knebel, J.-P. Brison, A. Pourret, D. Braithwaite, G. Lapertot, Q. Niu, M. Vališka, H. Harima, and J. Flouquet, Unconventional superconductivity in heavy fermion UTe_2, J. Phys. Soc. Jpn. **88**, 043702 (2019).

[24] T. Chen, H. Siddiquee, Z. Rehfuss, C. Lygouras, J. Drouin, S. Y. Gao, C. Lygouras, J. Drouin, V. Morano, K. E. Avers, C. J. Schmitt, A. Podlesnyak, S. Ran, Y. Song, and C. Broholm, Quasi-two-dimensional antiferromagnetic spin fluctuations in the spin-triplet in the spin-triplet superconductor candidate $CeRh_2As_2$, arXiv:2406.03566.

[25] R. Madar, P. Chaudouet, J. P. Senateur, S. Zemni, and D. Tranqui, New ternary pnictides with the $CaBe_2Ge_2$-type structure in the systems, rare-earth-Rh P and rare-earth-Rh As, J. Less-Common Met. **133**, 303 (1987).

[26] See Supplemental Material at http://link.aps.org/supplemental/10.1103/PhysRevB.110.L041120 for details of the DFT calculation and additional measurement data, and which includes Refs. [27–30].

[27] G. Kresse and J. Hafner, *Ab initio* molecular dynamics for liquid metals, Phys. Rev. B **47**, 558 (1993).

[28] G. Kresse and D. Joubert, From ultrasoft pseudopotentials to the projector augmented-wave method, Phys. Rev. B **59**, 1758 (1999).

[29] J. P. Perdew, K. Burke, and M. Ernzerhof, Generalized gradient approximation made simple, Phys. Rev. Lett. **77**, 3865 (1996).

[30] V. Wang, N. Xu, J. C. Liu, G. Tang, and W. T. Geng, VASPKIT: A user-friendly interface facilitating high-throughput computing and analysis using VASP code, Comput. Phys. Commun. **267**, 108033 (2021).

[31] Y. Wu, Y. J. Zhang, S. L. Ju, Y. Hu, G. W. Yang, H. Zheng, Y. A. Huang, Y. A. Zhang, H. L. Zhang, B. P. Song, N. C. Plumb, F. Steglich, M. Shi, G. Zwicknagl, C. Cao, H. Q. Yuan, and Y. Liu, Quasi-two-dimensional Fermi surface and heavy quasiparticles in $CeRh_2As_2$, arXiv:2309.06732v1.

[32] Y. Wu, Y. Zhang, S. Ju, Y. Hu, Y. Huang, Y. Zhang, H. Zhang, H. Zheng, G. Yang, E.-O. Eljaouhari, B. Song, N. C. Plumb, F. Steglich, M. Shi, G. Zwicknagl, C. Cao, H. Yuan, and Y. Liu, Fermi surface nesting with heavy quasiparticles in the locally noncentrosymmetric superconductor$CeRh_2As_2$, arXiv:2309.06732v2.

[33] X. Chen, L. Wang, J. Ishizuka, R. Zhang, K. Nogaki, Y. Cheng, F. Yang, Z. Chen, F. Zhu, Z. Liu, J. Mei, Y. Yanase, B. Lv, and Y. Huang, Coexistence of near-E_F flat band and van Hove singularity in a two-phase superconductor, Phys. Rev. X **14**, 021048 (2024).

[34] S. Patil, A. Generalov, M. Güttler, P. Kushwaha, A. Chikina, K. Kummer, T. C. Rödel, A. F. Santander-Syro, N. Caroca-Canales, C. Geibel, S. Danzenbächer, Y. Kucherenko, C. Laubschat, J. W. Allen, and D. V. Vyalikh, ARPES view on surface and bulk hybridization phenomena in the antiferromagnetic Kondo lattice $CeRh_2Si_2$, Nat. Commun. **7**, 11029 (2016).

[35] Y. H. Yuan, Y. X. Duan, J. Rusz, C. Zhang, J. J. Song, Q. Y. Wu, Y. Sassa, O. Tjernberg, M. Månsson, M. H. Berntsen, F. Y. Wu, S. Y. Liu, H. Liu, S. X. Zhu, Z. T. Liu, Y. Z. Zhao, P. H. Tobash, E. D. Bauer, J. D. Thompson, P. M. Oppeneer *et al.*, Angle-resolved photoemission spectroscopy view on the nature of Ce $4f$ electrons in the antiferromagnetic Kondo lattice $CePd_5Al_2$, Phys. Rev. B **103**, 125122 (2021).

[36] J. J. Song, Y. Luo, C. Zhang, Q. Y. Wu, T. Durakiewicz, Y. Sassa, O. Tjernberg, M. Månsson, M. H. Berntsen, Y. Z. Zhao, H. Liu, S. X. Zhu, Z. T. Liu, F. Y. Wu, S. Y. Liu, E. D. Bauer, J. Rusz, P. M. Oppeneer, Y. H. Yuan, Y. X. Duan *et al.*, The $4f$-hybridization strength in $Ce_mM_nIn_{3m+2n}$ heavy-fermion compounds studied by angle-resolved photoemission spectroscopy, Chin. Phys. Lett. **38**, 107402 (2021).

[37] Y. X. Duan, C. Zhang, J. Rusz, P. M. Oppeneer, T. Durakiewicz, Y. Sassa, O. Tjernberg, M. Månsson, M. H. Berntsen, F. Y. Wu, Y. Z. Zhao, J. J. Song, Q. Y. Wu, Y. Luo, E. D. Bauer, J. D. Thompson, and J. Q. Meng, Crystal electric field splitting and f-electron hybridization in heavy-fermion $CePt_2In_7$, Phys. Rev. B **100**, 085141 (2019).

[38] Q. Y. Chen, D. F. Xu, X. H. Niu, R. Peng, H. C. Xu, C. H. P. Wen, X. Liu, L. Shu, S. Y. Tan, X. C. Lai, Y. J. Zhang, H. Lee, V. N. Strocov, F. Bisti, P. Dudin, J.-X. Zhu, H. Q. Yuan, S. Kirchner, and D. L. Feng, Band dependent interlayer f-electron hybridization in $CeRhIn_5$, Phys. Rev. Lett. **120**, 066403 (2018).

[39] Q. Yao, D. Kaczorowski, P. Swatek, D. Gnida, C. H. P. Wen, X. H. Niu, R. Peng, H. C. Xu, P. Dudin, S. Kirchner, Q. Y. Chen, D. W. Shen, and D. L. Feng, Electronic structure and $4f$-electron character in Ce_2PdIn_8 studied by angle-resolved photoemission spectroscopy, Phys. Rev. B **99**, 081107(R) (2019).

[40] Y. Luo, C. Zhang, Q. Y. Wu, F. Y. Wu, J. J. Song, W. Xia, Y. Guo, J. Rusz, P. M. Oppeneer, T. Durakiewicz, Y. Z. Zhao, H. Liu, S. X. Zhu, Y. H. Yuan, X. F. Tang, J. He, S. Y. Tan, Y. B. Huang, Z. Sun, Y. Liu *et al.*, Three-dimensional and temperature-dependent electronic structure of the heavy-fermion compound $CePt_2In_7$ studied by angle-resolved photoemission spectroscopy, Phys. Rev. B **101**, 115129 (2020).

[41] Y. Wu, Y. Zhang, F. Du, B. Shen, H. Zheng, Y. Fang, M. Smidman, C. Cao, F. Steglich, H. Q. Yuan, J. D. Denlinger, and Y. Liu, Anisotropic c-f hybridization in the ferromagnetic quantum critical metal $CeRh_6Ge_4$, Phys. Rev. Lett. **126**, 216406 (2021).

[42] Q. Y. Chen, D. F. Xu, X. H. Niu, J. Jiang, R. Peng, H. C. Xu, C. H. P. Wen, Z. F. Ding, K. Huang, L. Shu, Y. J. Zhang, H. Lee, V. N. Strocov, M. Shi, F. Bisti, T. Schmitt, Y. B. Huang, P. Dudin, X. C. Lai, S. Kirchner *et al.*, Direct observation of how the heavy-fermion state develops in $CeCoIn_5$, Phys. Rev. B **96**, 045107 (2017).

[43] Y. Z. Zhao, J. J. Song, Q. Y. Wu, H. Liu, C. Zhang, B. Chen, H. Y. Zhang, Z. H. Chen, Y. B. Huang, X. Q. Ye, Y. H. Yuan, Y. X. Duan, J. He, and J. Q. Meng, Experimental observation of the significant difference between surface and bulk Kondo processes in Kondo lattice $YbCu_2Si_2$, Sci. China: Phys., Mech. Astron. **67**, 247413 (2024).

[44] S. Fujimori, Band structures of $4f$ and $5f$ materials studied by angle-resolved photoelectron spectroscopy, J. Phys.: Condens. Matter **28**, 153002 (2016).

[45] J. Q. Meng, P. M. Oppeneer, J. A. Mydosh, P. S. Riseborough, K. Gofryk, J. J. Joyce, E. D. Bauer, Y. Li, and T. Durakiewicz, Imaging the three-dimensional Fermi-surface pairing near the hidden-order transition in URu_2Si_2 using angle-resolved photoemission spectroscopy, Phys. Rev. Lett. **111**, 127002 (2013).

[46] X. Y. Ji, X. B. Luo, Q. Y. Chen, W. Feng, Q. Q. Hao, Q. Liu, Y. Zhang, Y. Liu, X. Y. Wang, S. Y. Tan, and X. C. Lai, Direct observation of coexisting Kondo hybridization and antiferromagnetic state in UAs_2, Phys. Rev. B **106**, 125120 (2022).

[47] J. J. Song, C. Zhang, Q. Y. Wu, Y. Z. Zhao, J. Rusz, J. J. Joyce, K. S. Graham, P. S. Riseborough, C. G. Olson, H. Liu, B. Chen, Y. H. Yuan, Y. X. Duan, P. H. Tobash, E. D. Bauer, P. M. Oppeneer, T. Durakiewicz, and J. Q. Meng, Relocalization of uranium $5f$ electrons in the antiferromagnetic heavy-fermion superconductor UPd_2Al_3: Insights from angle-resolved photoemission spectroscopy, Phys. Rev. B **109**, 205114 (2024).

[48] H. J. Im, T. Ito, H. D. Kim, S. Kimura, K. E. Lee, J. B. Hong, Y. S. Kwon, A. Yasui, and H. Yamagami, Direct observation of

dispersive Kondo resonance peaks in a heavy-fermion system, Phys. Rev. Lett. **100**, 176402 (2008).

[49] P. Coleman, Heavy electrons, in *Introduction to Many-Body Physics* (Cambridge University Press, Cambridge, UK, 2015), pp. 656–719.

[50] Z. Wu, Y. Fang, H. Su, W. Xie, P. Li, Y. Wu, Y. Huang, D. Shen, B. Thiagarajan, J. Adell, C. Cao, H. Q. Yuan, F. Steglich, and Y. Liu, Revealing the heavy quasiparticles in the heavy-fermion superconductor $CeCu_2Si_2$, Phys. Rev. Lett. **127**, 067002 (2021).